ChemComm

COMMUNICATION

View Article Online
View Journal | View Issue

Cite this: *Chem. Commun.*, 2014, **50**, 8757

Received 15th April 2014,
Accepted 16th June 2014

DOI: 10.1039/c4cc02767a

www.rsc.org/chemcomm

Targeted and image-guided photodynamic cancer therapy based on organic nanoparticles with aggregation-induced emission characteristics†

Youyong Yuan,‡[a] Guangxue Feng,‡[ab] Wei Qin,[c] Ben Zhong Tang[cd] and Bin Liu*[ae]

We report for the first time that organic nanoparticles with photodynamic activity and aggregation-induced emission characteristics are developed for targeted and image-guided photodynamic cancer therapy.

Image-guided delivery systems combining both medical diagnostics and therapeutics have received great attention for personalized medicine.[1] Among them, photodynamic therapy (PDT) has been proven to be one of the most elegant strategies for cancer therapy as the treatment can be readily regulated by a beam of light with noninvasive properties, precise controllability as well as high spatiotemporal precision.[2] PDT is based on the concept that photosensitizers (PSs) can generate toxic reactive oxygen species (ROS) capable of killing tumor cells upon exposure to light.[3] Meanwhile, upon light activation, PSs can also emit light for image-guided therapy.[4] Following the accumulation of the PSs in the target site monitored by fluorescence imaging, therapy can be precisely applied by selective irradiation with a beam of light. However, a common problem for PSs, especially the most widely used porphyrin derivatives, is that they could easily aggregate through π–π stacking due to their hydrophobic and rigid planar structures, resulting in aggregation caused fluorescence quenching[5] and dramatic reduction in ROS generation.[6] The situation is more severe when the PSs are encapsulated into nanocarriers, which result in significant reduction of their fluorescence and photodynamic activity.[7]

Aggregation-induced emission (AIE), an extraordinary phenomenon that is exactly opposite to the aggregation caused quenching effect, has emerged as a powerful and versatile tool for biological applications.[8] Propeller-shaped luminogens, such as tetraphenylethene (TPE) and silole derivatives, are nonemissive in the molecularly dissolved state but are induced to emit bright fluorescence by aggregation due to the restriction of intramolecular rotations (RIR) and prohibition of energy dissipation *via* non-radiative channels.[9] These unique properties make them particularly attractive for the development of AIE light-up bioprobes and AIE dots for biological sensing and imaging.[10] Although AIE luminogen has been used as an energy donor to enhance the ROS generation of porphyrin derivatives,[11] reports on AIE luminogens themselves or AIE nanoparticles for PDT have not yet been published. As aggregation is a natural process for most PSs, it is ideal if one could develop PSs that show enhanced fluorescence and phototoxicity upon aggregation formation.

In this contribution, we report for the first time that AIE nanoparticles (NPs) can be used for image-guided PDT. Using 2-(2,6-bis((*E*)-4-(phenyl(4′-(1,2,2-triphenylvinyl)-[1,1′-biphenyl]-4-yl)amino)styryl)-4*H*-pyran-4-ylidene)malononitrile (TTD) as an example, encapsulation of TTD using 1,2-distearoyl-*sn-glycero*-3-phosphoethanolamine-*N*-[maleimide(polyethylene glycol)] (DSPE-PEG-Mal) as the encapsulation matrix (Scheme 1), followed by surface functionalization with the target moiety of the cyclic arginine-glycine-aspartic acid (cRGD) tripeptide yielded the targeted TTD NPs (T-TTD NPs). The NPs can generate ROS efficiently and selectively to image and kill MDA-MB-231 cells upon light irradiation.

The photosensitizer TTD was synthesized according to our previous report.[9b] The TTD NPs were prepared by a nanoprecipitation method using DSPE-PEG-Mal as the encapsulation matrix. The hydrophobic DSPE segment will intertwine TTD to form the core, while hydrophilic PEG chains will render outside towards the water phase and provide the surface maleimide

[a] *Department of Chemical and Biomolecular Engineering, National University of Singapore, 4 Engineering Drive 4, Singapore 117576. E-mail: cheliub@nus.edu.sg*
[b] *Environmental Research Institute, National University of Singapore, Singapore 117411*
[c] *Department of Chemistry, Division of Biomedical Engineering, The Hong Kong University of Science and Technology, Clear Water Bay, Kowloon, Hong Kong*
[d] *SCUT–HKUST Joint Research Laboratory, Guangdong Innovative Research Team, State Key Laboratory of Luminescent Materials and Devices, South China University of Technology, Guangzhou, 510640, China*
[e] *Institute of Materials Research and Engineering, 3 Research Link, Singapore 117602*

† Electronic supplementary information (ESI) available: Detailed experimental methods and additional data. See DOI: 10.1039/c4cc02767a

‡ These authors contributed equally.

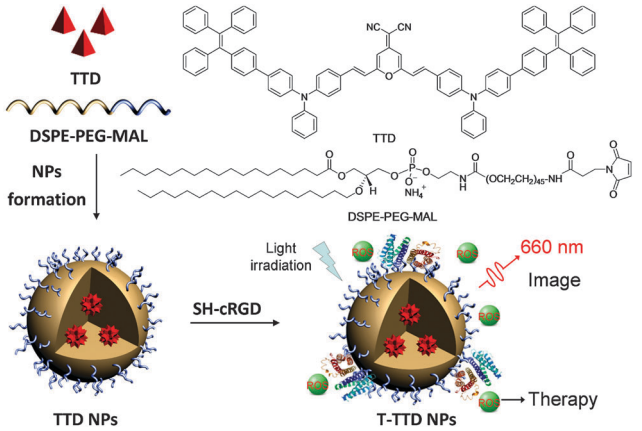

Scheme 1 Schematic illustration of T-TTD NP formation and surface modification with the target moiety of cRGD.

group for further conjugation. The obtained TTD NPs were further conjugated with cRGD-SH using click chemistry between the surface maleimide and -SH to yield the T-TTD NPs, which can specifically recognize cancer cells with overexpressed $\alpha_v\beta_3$ integrin. The hydrodynamic size distribution of T-TTD NPs was evaluated by dynamic light scattering (DLS). They have an average size of ~32 nm with a low polydispersity of ~0.12 (Fig. 1A). The morphology of the T-TTD NPs was examined by high-resolution transmission electron microscopy (HR-TEM), which shows spherical NPs with a mean size of ~30 nm. The UV-Vis and photoluminescence (PL) spectra of T-TTD NPs are shown in Fig. 1B. They have two absorption peaks centred at 353 and 502 nm, respectively, with an emission maximum peaked at 660 nm. It should be noted that the encapsulation of TTD in NPs

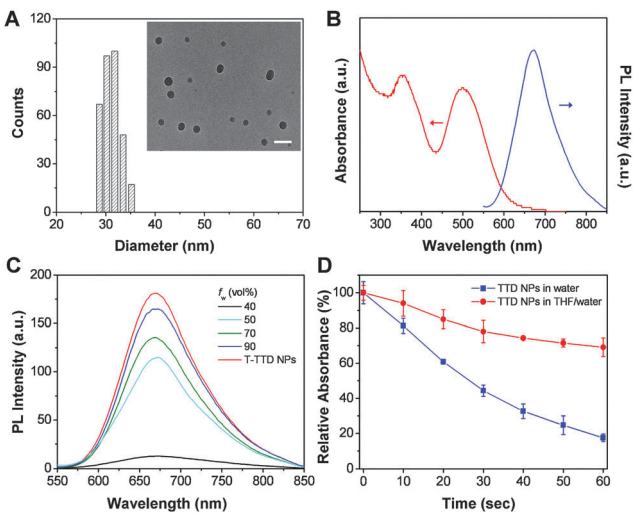

Fig. 1 (A) Size distribution and TEM image (inset) of T-TTD NPs. The scale bar is 100 nm. (B) UV-vis absorption and emission (λ_{ex} = 502 nm) spectra of T-TTD NPs. (C) PL spectra of 10 μM TTD (λ_{ex} = 502 nm) in THF–water mixtures at the same total volume with different water fractions (f_w) together with the PL spectrum of T-TTD NPs; (D) plots of the changes in absorbance of 1,3-diphenylisobenzofuran (DPBF) at 418 nm *vs.* irradiation time with T-TTD NPs in water or in the mixed solvent (THF/H_2O = 60/40, v/v). Data represent mean values ± standard deviation, n = 3.

and the NP size variation do not obviously affect the absorption and emission spectra of TTD (Fig. S1, ESI†). The fluorescence quantum yield was 10 ± 1%, measured using Rhodamine 6G in methanol as the standard.

The PL spectra of TTD in THF and water mixtures with different water fractions (f_w) are shown in Fig. S2 (ESI†) (f_w = 0 to 40%) and in Fig. 1C (f_w = 40 to 100%). TTD shows moderate fluorescence in THF. With gradual addition of water into THF (f_w = 0 to 40%), the emission of TTD is dramatically weakened and the emission color is bathochromically shifted, due to the increase in the solvent polarity and the transformation into the twisted intramolecular charge transfer state. The light emission is invigorated from f_w > 40 vol% and is intensified with a further increase in f_w, indicating that TTD is an AIE active luminogen.[9] When TTD is loaded into the polymer matrix, the TTD NPs show bright red fluorescence.

In general, for PSs, upon photoexcitation, intersystem crossing occurs from the singlet excited state to the triplet state, which is followed by interaction with molecular oxygen to yield ROS.[12] The ROS generation capability of T-TTD NPs in water and in the mixed solvents (THF/water = 60/40, v/v) was thus evaluated using 1,3-diphenylisobenzofuran (DPBF) as the indicator. DPBF can readily undergo 1,4-cycloaddition reaction with ROS to result in decreased absorbance at 418 nm.[13] As shown in Fig. 1D, upon exposure of the mixture of DPBE and T-TTD NPs to light irradiation for 1 minute, the 418 nm absorbance is decreased to 16.3% of its original value, indicative of efficient ROS generation. Under the same condition, when T-TTD NPs were dissolved in the mixed solvent (as fully dissolved molecules) the 418 nm absorbance decreases less than 30%. It should be noted that the absorbance of TTD at 418 nm does not contribute to the measured absorbance change due to its very low concentration (Fig. S3, ESI†). In addition, as the response of DPBF to ROS is inhibited by H_2O (Fig. S4, ESI†),[11b] the larger absorbance decrease for DPBF in T-TTD NP aqueous media than that in mixed solvent clearly demonstrates that TTD molecules can generate ROS more efficiently in the aggregated state.

To test the targeting effect of T-TTD NPs, MDA-MB-231 cancer cells with overexpressed $\alpha_v\beta_3$ integrin on the cellular membrane were chosen as integrin-positive cancer cells, while MCF-7 cancer cells and NIH 3T3 normal cells with low $\alpha_v\beta_3$ integrin expression were used as the negative controls. We incubated the T-TTD NPs with MDA-MB-231, MCF-7 and NIH 3T3 cells and the fluorescence of T-TTD NPs was monitored. The confocal images are shown in Fig. 2, where red fluorescence of T-TTD NPs in the cytoplasm and blue fluorescence of Hoechst from the cell nucleus are simultaneously observed in MDA-MB-231 cells after 1 h incubation. It is obvious that the red fluorescent signals in MCF-7 and NIH 3T3 cells are much weaker than that in MDA-MB-231 cells at different incubation time points (Fig. 2 and Fig. S5, ESI†). Receptor blocking experiments were also carried out to investigate the uptake mechanism of T-TTD NPs. In these experiments, free cRGD was first incubated with MDA-MB-231 cells before T-TTD NPs were added. As shown in Fig. S6 (ESI†), the red fluorescent signal of T-TTD NPs is dramatically reduced to about 30% of that shown

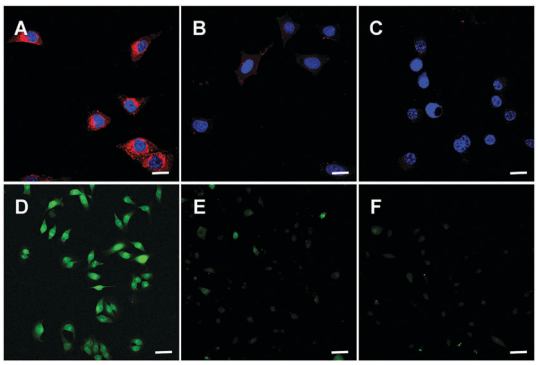

Fig. 2 (A–C) Confocal images of MDA-MB-231 (A), MCF-7 (B) and NIH 3T3 (C) cells after incubation with T-TTD NPs (1 μg mL^{-1}) for 1 h. The blue fluorescence from the nuclei of cells is dyed by Hoechst 33342, the red fluorescence is from T-TTD NPs. Images A–C share the same scale bar of 20 μm. (D–F) Detection of intracellular ROS production by dichlorofluorescein diacetate (DCF-DA) in MDA-MB-231 (D), MCF-7 (E) and NIH 3T3 (F) cells after incubation with T-TTD NPs (1 μg mL^{-1}) followed by light irradiation. Images D–F share the same scale bar of 50 μm.

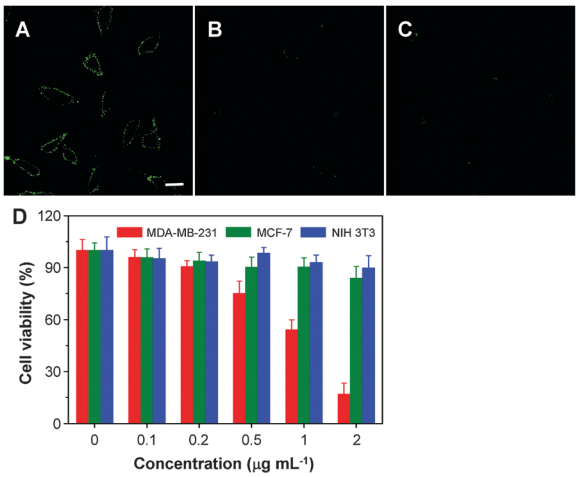

Fig. 3 Cell apoptosis imaging using FITC-tagged Annexin V in MDA-MB-231 (A), MCF-7 (B) and NIH 3T3 (C) cells incubated with T-TTD NPs after light irradiation. All images share the same scale bar of 20 μm. (D) Inhibition of growth of MDA-MB-231, MCF-7 and NIH 3T3 cells in the presence of different concentrations of T-TTD NPs with light irradiation (0.25 W cm^{-2}, 2 min) followed by further incubation of the cells for 24 h. Data represent mean values ± standard deviation, n = 3.

in Fig. 2A when the integrin is initially blocked with the excess cRGD. These results demonstrate that the T-TTD NPs were uptaken through $\alpha_v\beta_3$ integrin receptor-mediated endocytosis.

To evaluate the ROS production by T-TTD NPs after cancer cell uptake, we detected the ROS generation under light irradiation using a cell permeable fluorescent dye dichlorofluorescein diacetate (DCF-DA). DCF-DA was chosen as the ROS generation indicator, as it can be rapidly oxidized to highly fluorescence dichlorofluorescein (DCF) in the presence of ROS. As shown in Fig. 2D, strong green fluorescence of DCF was observed inside the cells, demonstrating efficient ROS generation from the T-TTD NPs. In contrast, negligible green fluorescence is observed when T-TTD NPs are incubated with MCF-7 (Fig. 2E) or NIH 3T3 (Fig. 2F) cells, which should be due to the ineffective cellular uptake of T-TTD NPs.

Apoptosis is the process of programmed cell death. Fluorescein isothiocyanate (FITC)-tagged Annexin V is one of the most commonly used fluorescent probes to distinguish viable cells from apoptotic ones. Annexin V can bind to the membrane of apoptotic cells which express phosphatidylserine. As shown in Fig. 3A, after incubating MDA-MB-231 cells with T-TTD NPs, followed by light irradiation, green fluorescence attributed to FITC is clearly observed from the cell membrane, indicating that the cells underwent the apoptosis process. No FITC signal is detectable in MCF-7 (Fig. 3B) and NIH 3T3 (Fig. 3C) cells, which agrees with the results shown in Fig. 2E and F. Further quantitative evaluation of the therapeutic effect of T-TTD NPs at different concentrations was studied by standard MTT assay. As shown in Fig. 3D, upon incubation of T-TTD NPs with MDA-MB-231, MCF-7 and NIH 3T3 cells, the NPs only show obvious cytotoxicity to MDA-MB-231 cells, with a half-maximal inhibitory concentration (IC_{50}) of 1.1 μg mL^{-1} under our experimental conditions. After the cells were illuminated with light at 0.25 W cm^{-2} for 2 minutes, quantitative analysis of cell viabilities for MDA-MB-231, MCF-7 and NIH 3T3 cells with different incubation time was also studied. As shown in Fig. S7 (ESI†), for MDA-MB-231, there is an obvious decrease in cell viability even within 4 hours, and the viability decreases with incubation time, reaching less than 15% in 24 hours. It should be noted that T-TTD NPs in the dark are non-toxic (Fig. S8, ESI†).

In summary, we fabricated AIE NPs with aggregation enhanced ROS generation for image-guided PDT. The AIE NPs show bright fluorescence and can effectively generate ROS under appropriate light irradiation. To selectively target a specific type of cancer cells, the cRGD peptide was conjugated to the NP surface. Cell viability studies showed that the T-TTP NPs could selectively and efficiently kill the cancer cells with overexpressed $\alpha_v\beta_3$ integrin. This PDT platform based on AIE luminogen is simple to design and synthesize, which offers new opportunities for image-guided PDT. Currently, we are working on the development of new AIE luminogen based PSs with near infrared absorption for *in vivo* applications.

We thank the Ministry of Defence (R279-000-340-232), the SMART (R279-000-378-592), and the Institute of Materials Research and Engineering of Singapore (IMRE/12-8P1103) for financial support.

Notes and references

1 K. Yang, L. Feng, X. Shi and Z. Liu, *Chem. Soc. Rev.*, 2013, **42**, 530–547.
2 J. F. Gohy and Y. Zhao, *Chem. Soc. Rev.*, 2013, **42**, 7117–7129.
3 D. E. Dolmans, D. Fukumura and R. K. Jain, *Nat. Rev. Cancer*, 2003, **3**, 380–387.
4 J. P. Celli, B. Q. Spring, I. Rizvi, C. L. Evans, K. S. Samkoe, S. Verma, B. W. Pogue and T. Hasan, *Chem. Rev.*, 2010, **110**, 2795–2838.
5 J. B. Birks, *Photophysics of Aromatic Molecules*, Wiley, 1970.
6 N. Sekkat, H. van den Bergh, T. Nyokong and N. Lange, *Molecules*, 2012, **17**, 98–144.
7 J. Moan, K. Berg and V. Iani, Action spectra of dyes relevant for photodynamictherapy, in *Photodynamic tumour therapy 2nd and 3rd generation photosensitizers*, ed. J. G. Moser, Harwood Academic Publishers, Amsterdam, 1998, pp. 1169–1181.

8 D. Ding, K. Li, B. Liu and B. Z. Tang, *Acc. Chem. Res.*, 2013, **46**, 2441–2453.
9 (*a*) Y. N. Hong, J. W. Y. Lam and B. Z. Tang, *Chem. Soc. Rev.*, 2011, **40**, 5361–5388; (*b*) W. Qin, D. Ding, J. Liu, W. Z. Yuan, Y. Hu, B. Liu and B. Z. Tang, *Adv. Funct. Mater.*, 2012, **22**, 771–779.
10 (*a*) X. Xue, Y. Zhao, L. Dai, X. Zhang, X. Hao, C. Zhang, S. Huo, J. Liu, C. Liu, A. Kumar, W. Q. Chen, G. Zou and X. J. Liang, *Adv. Mater.*, 2014, **26**, 712–717; (*b*) Y. Yuan, R. T. Kwok, B. Z. Tang and B. Liu, *J. Am. Chem. Soc.*, 2014, **136**, 2546–2554; (*c*) Y. Li, Y. Wu, J. Chang, M. Chen, R. Liu and F. Li, *Chem. Commun.*, 2013, **49**, 11335–11337; (*d*) Y. Yuan, R. T. Kwok, G. Feng, J. Liang, J. Geng, B. Z. Tang and B. Liu, *Chem. Commun.*, 2014, **50**, 295–297; (*e*) X. Huang, X. Gu, G. Zhang and D. Zhang, *Chem. Commun.*, 2012, **48**, 12195–12197; (*f*) H. Shi, R. T. K. Kwok, J. Liu, B. Xing, B. Z. Tang and B. Liu, *J. Am. Chem. Soc.*, 2012, **134**, 17972–17981.
11 (*a*) C. C. Chang, M.-C. Hsieh, J.-C. Lin and T.-C. Chang, *Biomaterials*, 2012, **33**, 897–906; (*b*) M.-C. Hsieh, C.-H. Chien, C. C. Chang and T.-C. Chang, *J. Mater. Chem. B*, 2013, **1**, 2350–2357.
12 A. P. Castano, T. N. Demidova and M. R. Hamblin, *Photodiagn. Photodyn. Ther.*, 2004, **1**, 279–293.
13 X. F. Zhang and X. Li, *J. Lumin.*, 2011, **131**, 2263–2266.

